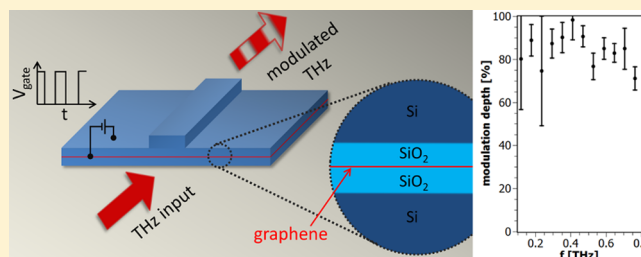


Graphene-Based Waveguide-Integrated Terahertz Modulator

Martin Mittendorff,^{*,†} Shanshan Li,^{†,‡} and Thomas E. Murphy^{†,‡}[†]Institute for Research in Electronics & Applied Physics and [‡]Department of Electrical & Computer Engineering, University of Maryland, College Park, Maryland 20742, United States

ABSTRACT: One of the major difficulties in the development of optoelectronic THz modulators is finding an active material that allows for large modulation depth. Graphene is a promising candidate because in the terahertz regime it behaves as a Drude metal with conductivity that can be electrostatically tuned through the application of a gate voltage. However, the maximum absorption incurred when a terahertz signal passes through a monolayer of graphene is still only on the order of 10–20%, even for the highest practically achievable carrier concentrations. We demonstrate here a THz modulator that overcomes this fundamental limitation by incorporating a graphene sheet on the surface of a passive silicon dielectric waveguide, in which the evanescent field penetrates the graphene sheet. By applying a gate voltage to the graphene sheet, a modulation depth of up to 50% was achieved. The performance of the modulator is confirmed through electromagnetic simulations, which give further insights into the spatial structure of the guided mode and polarization dependence of the modulation. We show both theoretically and experimentally that the modulation depth can be increased to over 90% by integrating the graphene sheet at the center of the waveguide.

KEYWORDS: graphene, terahertz photonics, terahertz modulator, terahertz waveguide



In recent years, there has been significant progress in developing new optoelectronic emitters and detectors that operate in the THz gap between the microwave and infrared regimes.^{1–5} Despite this, there are comparatively few methods to electrically modulate or switch a THz wave, a critical requirement in many proposed THz communication systems. Bulk photoconductive modulators, in which photo-generated carriers modulate the conductivity of a semiconductor, have achieved a modulation depth above 99% in germanium, but such systems typically require an intense optical pulse and the response time is determined by the carrier lifetime.⁶ This approach does not easily translate to the electrical regime because it is impossible to volumetrically inject electrons into a bulk semiconductor by purely electrical means. For this reason, the most common materials used for electrical terahertz modulation are two-dimensional conductors, such as quantum wells or graphene sheets. The limited light–matter interaction in a thin two-dimensional film makes it difficult to simultaneously achieve a high modulation depth and broad terahertz bandwidth. A fast modulator based on quantum wells that allowed for a modulation depth of 3% was described in 2004.⁷ One way to improve the modulation depth (at the expense of terahertz bandwidth) is by introducing metamaterial structures, which provide resonant enhancement of the absorption at specific terahertz frequencies. Chen et al.⁸ demonstrated a THz modulator based on this principle that achieved a modulation depth of 50%. Graphene has recently emerged as a promising alternative to traditional semiconductor two-dimensional electron gas, with potential optoelectronic applications.^{9–11} Its high charge carrier mobility allows more

efficient modulation of THz radiation of up to 15% at normal incidence,¹² and its mechanical properties enable the development of flexible modulators.¹³ Again, the modulation depth can be strongly enhanced to about 80% by combining the graphene sheet with a metamaterial or plasmonic structure.^{14,15} A recent study presents a THz modulator based on a plasmonic structure on top of a semiconductor heterostructure¹⁶ that reached a modulation depth of 85% at a modulation frequency of 1 GHz. Higher modulation efficiencies can be achieved if a graphene sheet is incorporated into the lasing cavity.¹⁷ While the metamaterial and plasmonic structures enable a high modulation depth, the terahertz frequency range is fundamentally limited to a small range around the plasmonic resonance.

Another way to increase the light–matter interaction is to guide the radiation along a graphene sheet, e.g., in a waveguide. This principle has been exploited for near-infrared detectors and modulators.^{18–20} Two very recent articles discuss theoretically a graphene-based modulator based on a THz waveguide. Locatelli et al. propose a waveguide structure with graphene on top as well as a coupler with a graphene sheet between two waveguides to modulate the coupling efficiency.²¹ Xiao et al. present a different solution by integrating the graphene into a plasmonic waveguide.²² Here we present a THz modulator based on a large-area graphene sheet in combination with a dielectric waveguide. With this combination we achieved a broadband modulation depth of around 90%. The experimental measurements are verified by numerical

Received: September 29, 2016

Published: January 5, 2017

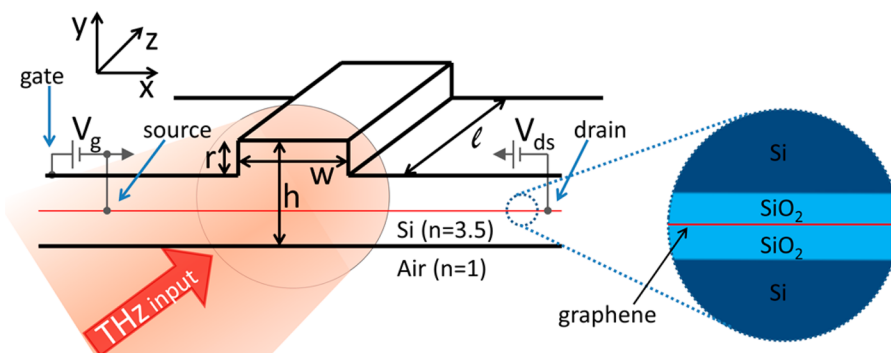


Figure 1. Sketch of the waveguide structure. The THz beam is focused to the front facet of the dielectric waveguide; a graphene sheet serves as tunable absorber to modulate the THz radiation. The gate contact is connected to the Si; source and drain are connected to the graphene layer.

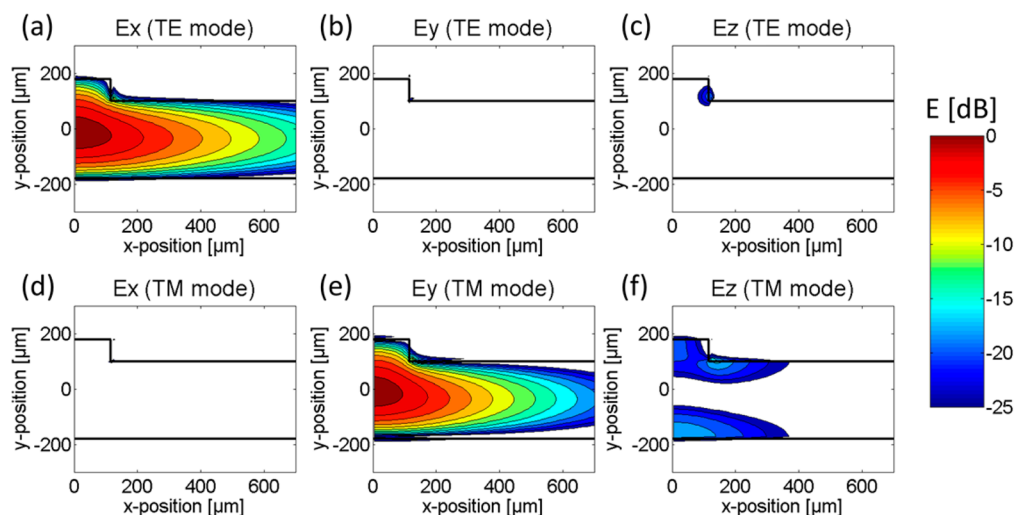


Figure 2. Calculated electric field components in x (a, d), y (b, e), and z (c, f) directions of the fundamental TE (a, b, c) and TM (d, e, f) modes for a silicon waveguide with an overall thickness of $355\ \mu\text{m}$ and a ridge height of $80\ \mu\text{m}$ at a frequency of $1\ \text{THz}$. Only one-half of the waveguide is shown; the second half is symmetric to the plotted one. In order to easily distinguish the TM modes from the spurious modes of the finite computational window, we added an artificial 5% anisotropy to the silicon core region.

calculations, which predict the optimal placement of the graphene layer within the waveguide and polarization dependence of the modulator.

Modes in Dielectric Waveguides. The modulators presented in this work are based on a dielectric ridge waveguide depicted in Figure 1. Lightly p-doped Si serves as substrate material for the waveguide. A graphene sheet is either attached to the bottom of the waveguide or sandwiched in the center of the waveguide, with an intervening $300\ \text{nm}$ thick SiO_2 layer to allow for electrostatic modulation. The electric field of the THz radiation that is guided through the waveguide penetrates the graphene sheet and causes free-carrier absorption in the graphene sheet. Two electrical contacts are made to the graphene sheet, and a third contact to the lightly doped Si is used to apply a gate voltage. Applying a gate voltage between the graphene and silicon changes the carrier concentration in the graphene sheet²³ and therewith modulates the free-carrier absorption.

To analyze the distribution of the electric field for the fundamental TE and TM modes in a dielectric waveguide, we performed simulations using a full-vectorial optical-mode solver.²⁴ For these calculations, we assumed a dielectric waveguide with a total thickness of $h = 355\ \mu\text{m}$, a ridge height of $r = 80\ \mu\text{m}$, and a ridge width of $w = 230\ \mu\text{m}$. Highly resistive silicon with a refractive index of 3.5 was considered as waveguide material. The results of the calculation performed for

a frequency of $1\ \text{THz}$ are shown in Figure 2. The electric field components of the TE mode, which is excited by horizontally polarized THz radiation, are shown in Figure 2a–c. Figure 2d–f represent the electric field components for the TM mode, which is excited by vertically polarized radiation. While the TE mode provides only electrical fields in the x direction (cf. Figure 2a), the TM mode contains electrical field components in the y (cf. Figure 2e) and z (cf. Figure 2f) directions. In order to achieve absorption in a two-dimensional electron gas (2DEG), an in-plane field component is necessary.²⁵ Both TE and TM modes provide in-plane fields at the lower edge of the waveguide. While the electric field for the TE mode is aligned along the x axis, the in-plane component of the field for the TM mode is oriented along the z axis.

Calculations of the field distribution within the xz plane for two different positions are presented in Figure 3. The field distribution in the center (lower edge) of the waveguide is shown in Figure 3a (Figure 3c) and Figure 3b (Figure 3d) for the TE and the TM mode, respectively. For the cut at the lower edge of the waveguide, the field strengths of the TE and TM modes are similar, indicating polarization-independent modulation can be achieved. In contrast to that, the field strength of the TE mode in the center of the waveguide (cf. Figure 3a) is larger by about 1 order of magnitude (note the different scale bars), indicating the optimal position of a 2DEG for an

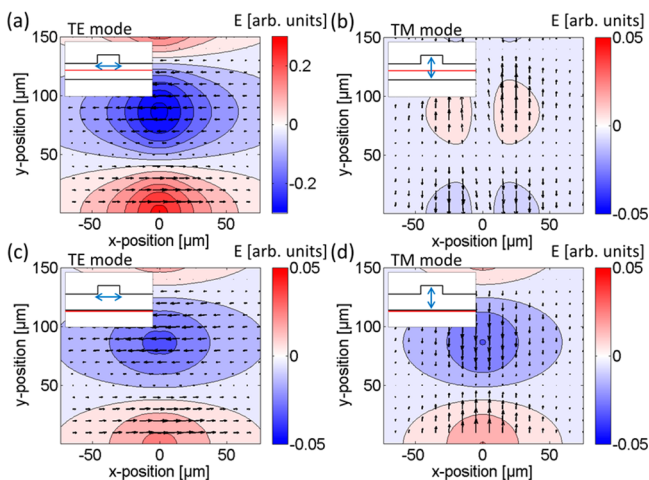


Figure 3. Calculated distribution of the electric field at the lower edge and the center of the waveguide. The red line in the inset indicates the y position of the shown xz planes; the double arrows in the inset indicate the polarization of the transversal electrical field. The arrows in the main plots indicate the orientation of the electric field.

efficient modulator. At the same time, the field for the TM mode is nearly absent in this plane (cf. Figure 3b).

Device Fabrication and Experimental Results. Two different types of modulators were fabricated to experimentally prove the concept of a waveguide-integrated THz modulator: A simpler device with the graphene on the lower edge of the waveguide and a more complex device, consisting of a silicon sandwich with a graphene layer in its center (cf. Figure 1). Both waveguides employ lightly doped silicon with a conductivity of about $250 \text{ } \Omega\text{cm}$ and are similar to the ones presented in ref 26. The light doping is low enough to minimize the terahertz absorption coefficient of the silicon while at the same time allowing for the electrostatic gating of the graphene.

Two different methods were employed to produce ridges with a height of about $r = 100 \text{ } \mu\text{m}$: deep reactive-ion etching and milling with a dicing saw. A 300 nm thick thermal oxide on the silicon serves as a gate dielectric. Large-area graphene grown by chemical vapor deposition (CVD) on copper was transferred to the waveguide with poly(methyl methacrylate) (PMMA).²⁷ The graphene covers an area of about $8 \times 8 \text{ mm}^2$, and the length of the waveguide is $l = 10 \text{ mm}$. Source and drain contacts were added to the graphene with conductive epoxy far from the ridge, and a third contact for gating was made to the Si substrate. The front facets of the two devices are shown in Figure 4a and b. The device shown in Figure 4a features a ridge height of $r = 80 \text{ } \mu\text{m}$ and a width of $w = 230 \text{ } \mu\text{m}$, and the overall height of the device is $h = 355 \text{ } \mu\text{m}$, with the graphene sheet placed on the lower edge of the waveguide. The second device (shown in Figure 4b) features a ridge height of $r = 160 \text{ } \mu\text{m}$ and a width of $w = 150 \text{ } \mu\text{m}$, and the overall height of this device is $h = 550 \text{ } \mu\text{m}$. The graphene sheet (cf. the horizontal line in Figure 4b) in this device is sandwiched between two silicon wafers; the patterning of the ridge in the upper part was done before assembling the waveguide. To achieve mechanical bonding, dissolved PMMA was applied at the interface edge between two facing wafers, whereupon capillary forces draw the PMMA solution into the small gap between the wafers.

Electrically, the modulators function as large-area field-effect transistors; a typical gating curve is shown in Figure 4c. As the dc conductivity changes by applying a gate voltage, so too is the

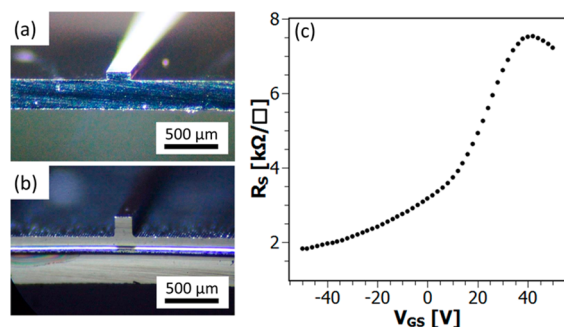


Figure 4. Optical micrographs of the waveguide with the graphene on the lower edge (a) and in the center of the waveguide (b). (c) Sheet resistance as a function of the gate voltage of one of the waveguide shown in part (b).

free-carrier absorption varied, resulting in modulation of the guided THz radiation.

To determine the performance of the two devices, a standard THz time-domain spectroscopy setup was employed. A femto-second laser working at a center wavelength of 800 nm is used to pump a large-area THz emitter.²⁸ The THz radiation is collimated and refocused to the input facet of the waveguide by a pair of two off-axis parabolic mirrors. A second pair off-axis parabolic mirrors is used to collect the radiation that passed through the waveguide and refocus it to a ZnTe crystal for recording the THz transient via electro-optic sampling. To measure the TE (TM) mode of the waveguide, the electric field of the THz radiation was polarized horizontally (vertically). While the THz pulse without waveguide is a single-cycle pulse, the waveguide dispersion leads to a chirp of the THz pulse (cf. inset in Figure 5a). Fourier transform of the THz transient reveals the spectral content of the pulse (cf. Figure 5a), which is

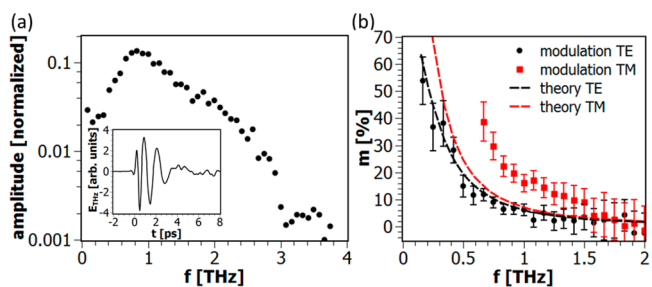


Figure 5. (a) Amplitude spectrum of the THz pulse that passed through the waveguide at a gate voltage of -35 V . The inset shows the corresponding THz transient. (b) Measured (points) and calculated (dashed lines) modulation depth as a function of frequency for TE and TM modes for a gate voltage of $\pm 35 \text{ V}$.

recorded for different gate voltages. The amplitude spectrum is normalized to the amplitude without the waveguide at 1 THz . Introducing the waveguide into the setup decreased the amplitude at 1 THz to about 12% of its initial value. This decrease is caused by three main effects: the Fresnel reflection at input and output facets, the coupling of the incoming THz radiation to the waveguide mode, and the attenuation of the waveguide itself. We estimate the losses in THz power from Fresnel reflection to be around 31% for each of the Si air interfaces, and the coupling efficiency to the waveguide was estimated by the calculated mode area and the THz spot size to be around 10%. The attenuation of the THz power caused by free-carrier absorption of the waveguide was estimated to be around 50%.²⁶

These three contributions add up to an overall decrease of the power to 2.4%, corresponding to a decrease in THz field to 15%, which is in good agreement with the measured value. The modulation depth is calculated from the power spectra $P(\omega)$ via $m(\omega) = (P(\omega)_{\max} - P(\omega)_{\min})/P(\omega)_{\max}$. The result of the waveguide with the graphene on the lower edge (cf. Figure 4 a) is shown in Figure 5b. With this simple approach a modulation depth of up to 50% is reached at 0.2 THz when the gate voltage is varied between -35 and 35 V. The modulation depth decreases significantly with increasing frequency and drops below 10% for frequencies above 1.5 THz. Time-domain spectroscopy provides information not only about the amplitude and power spectrum but also about the phase of the spectral content. Comparing the phase of the two THz spectra obtained at ± 35 V gate voltage, we observed a rather small modulation of about 4° over the 10 mm waveguide length at a frequency of 0.7 THz.

To simulate the modulation with the mode solver, we included a conductive sheet with a thickness of 25 nm. The far-infrared properties of the graphene can be well described by the Drude model,²⁹ which includes the dc conductivity σ_{dc} and the scattering time τ . At $+35$ V (35 V) gate voltage, the source–drain resistivity in both devices is about 6 k Ω (1.6 k Ω), which corresponds to a 25 nm thick layer with a dc conductivity of 6.7 kS/m (25 kS/m). The complex conductivity $\sigma(\omega)$ of the conductive sheet at THz frequencies is calculated via $\sigma(\omega) = \frac{\sigma_{\text{dc}}}{1 + i\omega\tau}$. For our calculations we assumed a carrier relaxation time of $\tau = 10$ fs,³⁰ corresponding to a carrier mobility of about 400 cm²/(V s). Even though the thickness of the conductive layer in the numerical model is much larger than the actual thickness of a graphene layer, it is far smaller than the wavelength of the THz radiation and can be still considered as 2DEG for the THz radiation. This was verified via calculations with varied layer thickness that did not show significant changes of the simulation results. The lightly doped Si was considered to be loss-free with a refractive index of 3.5. The mode solver calculates the field distribution of the fundamental TE and TM modes, as well as the effective refractive index, including the imaginary part representing the loss in the waveguide. From the effective refractive index, we calculated the transmission through a 10 mm long waveguide for gate voltages of -35 and 35 V and subsequently the modulation depth. The results agree well with the obtained experimental data (cf. dashed lines in Figure 5b). The fast drop-off of the modulation depth with increasing frequency is attributed to the stronger field confinement, which leads to a smaller evanescent field penetrating the graphene sheet at higher frequencies. The TE mode is more strongly confined than the TM mode, which leads to a lower modulation depth compared to the TM mode (cf. Figure 3c and d). The measured modulation depth for the TM eigenstate was observed to be stronger than that of the TE eigenstate, an effect that is underestimated by theory. A likely explanation for this discrepancy is that measurements used electro-optic sampling of the field emerging from the waveguide, which is susceptible to electrically induced shifts in the optical mode profile and leakage into cladding modes, effects that are not incorporated into the simple theoretical model. As the confinement of the mode decreases with wavelength, the acceptance angle for the free space coupling of the THz radiation becomes diminished; this is the reason for the lack of experimental data below 0.6 THz for the TE mode. Hence, the dimensions of the waveguide dictate the frequency range in which the modulation works well. The low phase

modulation observed in the experiment is also reproduced by the model: While the imaginary part of the calculated effective refractive index for the TE mode changes from 1.4×10^{-4} to 5.3×10^{-4} at 0.7 THz, the real part changes from 3.44154 to 3.44155, corresponding to a phase change below 1° over 10 mm.

Placing the graphene sheet in the center of the device strongly increases the modulation depth, as shown in Figure 6 a.

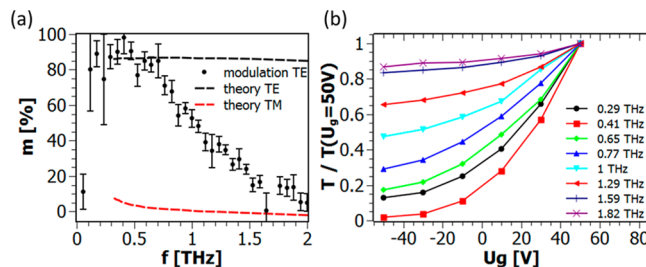


Figure 6. (a) Experimental and theoretical results for the modulation of the THz waveguide with the centered graphene sheet (cf. Figure 4b). (b) Normalized gate-voltage dependence of the transmission through the waveguide for various frequencies.

As the device dimensions of this sandwich structure are larger, the low-frequency components of the THz pulse are well guided. The modulation depth of the TE mode of this device reaches about 90% in a large frequency range spanning from 0.2 to 0.7 THz. While the simulations predict a constant modulation depth of 90%, the experimental data show a decrease in the modulation depth for frequencies above 0.7 THz. We attribute this discrepancy to the fact that, because of the larger dimensions, the waveguide supports multiple bound modes at higher frequencies, whereas only the fundamental mode was taken into account in the simulations. As expected from the calculation of the TM mode, only minor modulation of below 20% was observed in the experiments (not shown).

As with the waveguide with the graphene sheet on the edge, the phase modulation is rather small, reaching its maximum of about 30° at 0.7 THz. The phase change in the experiment is again close to the calculated phase modulation of 9° over a 10 mm waveguide length at 0.7 THz. Figure 6b shows the gate-voltage dependence of the transmission through the waveguide normalized to the transmission at 50 V, for frequencies ranging from 0.3 to 1.8 THz. This gate voltage dependence reproduces the gate-dependent resistance of the graphene sheet as presented in Figure 4c.

To estimate the highest modulation speed achievable with our device, we applied a rectangular shaped ac voltage to the gate and used a lock-in amplifier synchronized to the gate voltage for detection. This measurement revealed a cutoff frequency of about 2 kHz. This low cutoff frequency is caused by the large resistive-capacitive (RC) time constant of the device due to the high resistive substrate in combination with the large area of the device. Assuming a simple plate capacitor, we can estimate the capacitance of the device from its geometry, namely, the size of the graphene-covered area and the oxide thickness, to be about 11 nF. This, in combination with a resistance of 10 k Ω , derived from the conductivity and geometry of the Si substrate, leads to an RC time constant of about 0.1 ms, which is in agreement with the measured cutoff frequency.

DISCUSSION

For waveguide modulators and detectors in the visible and near-infrared regime, a strong increase of the device modulation

efficiency is predicted by inserting the graphene sheet into the core of the waveguide.³¹ While it is difficult to incorporate a graphene sheet into the core of a waveguide in the short-wavelength regime, it is rather straightforward to use such an approach in the THz range. With our approach we reached a modulation depth of about 90% in a spectral range spanning more than two octaves from 0.15 to 0.7 THz, proving that our modulator concept has a large potential for future applications. The modulation speed of a waveguide-based modulator is naturally limited by the optical length of the active region: after the absorption within the active area was changed, the radiation has to travel through the entire region before the maximum change is achieved. In our case with an active length of about 10 mm, this limit is about 5 GHz. Using a traveling wave structure for gating the graphene could allow modulation speeds beyond this limit. In such a device, the gate voltage would be traveling along the Si waveguide in a coplanar waveguide that allows matching of the propagation velocity between the THz radiation and the gate voltage. A similar device has been presented for near-infrared modulation beyond the transition time limit.³² However, due to the large RC time constant of about 0.1 ms, our device is far below this value. Significant improvement of the modulation speed could be achieved by employing two layers of high-mobility graphene that are separated by a thin dielectric material, e.g., Al₂O₃.^{33,34} This would reduce the resistivity and therewith the RC time constant, allowing faster modulation. A thinner oxide would also decrease the gate voltage needed to achieve a strong modulation to feasible values of below ± 5 V.³⁵ In addition, this would also allow using a silicon substrate with higher resistivity, which would decrease the minimum losses and therewith further improve the modulation depth. In an optimized single-mode waveguide with dispersion compensation, the highest modulation frequency is ultimately limited by the mobility of the graphene. Recent measurements with high-mobility graphene suggest that operation in the THz range is possible.³⁶ Shrinking the size of the waveguide to reach a single-mode limit will extend the bandwidth to higher frequencies.

CONCLUSION

We present two different approaches to fabricate a waveguide-integrated graphene-based THz modulator. While the performance of the simple device, where the graphene sheet is penetrated only by the evanescent field, is mainly limited to frequencies that are only weakly confined, the more complex structure with the graphene sheet in the center of the mode reaches a high modulation depth of around 90% in a large frequency range between 0.15 and 0.7 THz. Simulations based on an optical mode solver for dielectric waveguides were employed to calculate the expected device performance; the simulations reproduced the experimental findings very well.

AUTHOR INFORMATION

Corresponding Author

*E-mail: Martin@Mittendorff.email

ORCID

Martin Mittendorff: 0000-0003-3998-2518

Notes

The authors declare no competing financial interest.

ACKNOWLEDGMENTS

We gratefully acknowledge funding from U.S. ONR (N000141310865) and the U.S. NSF (ECCS 1309750). The sample fabrication was carried out at the University of Maryland Nanocenter.

REFERENCES

- (1) Tonouchi, M. Cutting-edge terahertz technology. *Nat. Photonics* **2007**, *1*, 97–105.
- (2) Welp, U.; Kadowaki, K.; Kleiner, R. Superconducting emitters of THz radiation. *Nat. Photonics* **2013**, *7*, 702–710.
- (3) Vijayraghavan, K.; Jiang, Y.; Jang, M.; Jiang, A.; Choutagunta, K.; Vizbaras, A.; Demmerle, F.; Boehm, G.; Amann, M. C.; Belkin, M. A. Broadly tunable terahertz generation in mid-infrared quantum cascade lasers. *Nat. Commun.* **2013**, *4*, 2021.
- (4) Cai, X.; Sushkov, A. B.; Suess, R. J.; Jadidi, M. M.; Jenkins, G. S.; Nyakiti, L. O.; Myers-Ward, R. L.; Li, S.; Yan, J.; Gaskill, D. K.; Murphy, T. E.; Drew, H. D.; Fuhrer, M. S. Sensitive room-temperature terahertz detection via the photothermoelectric effect in graphene. *Nat. Nanotechnol.* **2014**, *9*, 814–819.
- (5) Mittendorff, M.; Kamann, J.; Eroms, J.; Weiss, D.; Drexler, C.; Ganichev, S. D.; Kerbusch, J.; Erbe, A.; Suess, R. J.; Murphy, T. E.; Chatterjee, S.; Kolata, K.; Ohser, J.; König-Otto, J. C.; Schneider, H.; Helm, M.; Winnerl, S. Universal ultrafast detector for short optical pulses based on graphene. *Opt. Express* **2015**, *23*, 28728–28735.
- (6) Schmidt, J.; Winnerl, S.; Seidel, W.; Bauer, C.; Gensch, M.; Schneider, H.; Helm, M. Single-pulse picking at kHz repetition rates using a Ge plasma switch at the free-electron laser FELBE. *Rev. Sci. Instrum.* **2015**, *86*, 063103.
- (7) Kleine-Ostmann, T.; Dawson, P.; Pierz, K.; Hein, G.; Koch, M. Room-temperature operation of an electrically driven terahertz modulator. *Appl. Phys. Lett.* **2004**, *84*, 3555–3557.
- (8) Chen, H.-T.; Padilla, W. J.; Zide, J. M. O.; Gossard, A. C.; Taylor, A. J.; Averitt, R. D. Active terahertz metamaterial devices. *Nature* **2006**, *444*, 597–600.
- (9) Bonaccorso, F.; Sun, Z.; Hasan, T.; Ferrari, A. C. Graphene photonics and optoelectronics. *Nat. Photonics* **2010**, *4*, 611–622.
- (10) Bao, Q.; Ping Loh, K. Graphene Photonics, Plasmonics, and Broadband Optoelectronic Devices. *ACS Nano* **2012**, *6*, 3677–3694.
- (11) Koppens, F. H. L.; Mueller, T.; Avouris, Ph.; Ferrari, A. C.; Vitiello, M. S.; Polini, M. Photodetectors based on graphene, other two-dimensional materials and hybrid systems. *Nat. Nanotechnol.* **2014**, *9*, 780–793.
- (12) Sensale-Rodriguez, B.; Yan, R.; Kelly, M. M.; Fang, T.; Tahy, K.; Hwang, W. S.; Jena, D.; Liu, L.; Xing, H. G. Broadband graphene terahertz modulators enabled by intraband transitions. *Nat. Commun.* **2012**, *3*, 780.
- (13) Liu, J.; Li, P.; Chen, Y.; Song, X.; Mao, Q.; Wu, Y.; Qi, F.; Zheng, B.; He, J.; Yang, H.; Wen, Q.; Zhang, W. Flexible terahertz modulator based on coplanar gate graphene field-effect transistor structure. *Opt. Lett.* **2016**, *41*, 816–819.
- (14) Lee, S. H.; Choi, M.; Kim, T.-T.; Lee, S.; Liu, M.; Yin, X.; Choi, H. K.; Lee, S. S.; Choi, C.-G.; Choi, S.-Y.; Zhang, X.; Min, B. Switching terahertz waves with gate-controlled active graphene metamaterials. *Nat. Mater.* **2012**, *11*, 936–941.
- (15) Gao, W.; Shu, J.; Reichel, K.; Nickel, D. V.; He, X.; Shi, G.; Vajtai, R.; Ajayan, P. M.; Kono, J.; Mittleman, D. M.; Xu, Q. High-Contrast Terahertz Wave Modulation by Gated Graphene Enhanced by Extraordinary Transmission through Ring Apertures. *Nano Lett.* **2014**, *14*, 1242–1248.
- (16) Zhang, Y.; Qiao, S.; Liang, S.; Wu, Z.; Yang, Z.; Feng, Z.; Sun, H.; Zhou, Y.; Sun, L.; Chen, Z.; Zou, X.; Zhang, B.; Hu, J.; Li, S.; Chen, Q.; Li, L.; Xu, G.; Zhao, Y.; Liu, S. Gbps Terahertz External Modulator Based on a Composite Metamaterial with a Double-Channel Heterostructure. *Nano Lett.* **2015**, *15*, 3501–3506.
- (17) Liang, G.; Hu, X.; Yu, X.; Shen, Y.; Li, L. H.; Davies, A. G.; Linfield, E. H.; Liang, H. K.; Zhang, Y.; Yu, S. F.; Wang, Q. J.

Integrated Terahertz Graphene Modulator with 100% Modulation Depth. *ACS Photonics* **2015**, *2*, 1559–1566.

(18) Gan, X.; Shiue, R.-J.; Gao, Y.; Meric, I.; Heinz, T. F.; Shepard, K.; Hone, J.; Assefa, S.; Englund, D. Chip-integrated ultrafast graphene photodetector with high responsivity. *Nat. Photonics* **2013**, *7*, 883–887.

(19) Liu, M.; Yin, X.; Ulin-Avila, E.; Geng, B.; Zentgraf, T.; Ju, L.; Wang, F.; Zhang, X. A graphene-based broadband optical modulator. *Nature* **2011**, *474*, 64–67.

(20) Youngblood, N.; Anugrah, Y.; Ma, R.; Koester, S. J.; Li, M. Multifunctional Graphene Optical Modulator and Photodetector Integrated on Silicon Waveguides. *Nano Lett.* **2014**, *14*, 2741–2746.

(21) Locatelli, A.; Town, G. E.; De Angelis, C. Graphene-Based Terahertz Waveguide Modulators. *IEEE Trans. Terahertz Sci. Technol.* **2015**, *5*, 351–357.

(22) Xiao, B.; Sun, R.; He, J.; Qin, K.; Kong, S.; Chen, J.; Xiumin, W. A Terahertz Modulator Based on Graphene Plasmonic Waveguide. *IEEE Photonics Technol. Lett.* **2015**, *27*, 2190–2192.

(23) Novoselov, K. S.; Geim, A. K.; Morozov, S. V.; Jiang, D.; Zhang, Y.; Dubonos, S. V.; Grigorieva, I. V.; Firsov, A. A. Electric Field Effect in Atomically Thin Carbon Films. *Science* **2004**, *306*, 666–669.

(24) Fallahkhair, A. B.; Li, K. S.; Murphy, T. E. Vector Finite Difference Modesolver for Anisotropic Dielectric Waveguides. *J. Lightwave Technol.* **2008**, *26*, 1423–1431.

(25) Kovacevic, G.; Yamashita, S. Waveguide design parameters impact on absorption in graphene coated silicon photonic integrated circuits. *Opt. Express* **2016**, *24*, 3584–3591.

(26) Li, S.; Kumar, G.; Murphy, T. E. Terahertz nonlinear conduction and absorption saturation in silicon waveguides. *Optica* **2015**, *2*, 553–557.

(27) Li, X.; Zhu, Y.; Cai, W.; Borysiak, M.; Han, B.; Chen, D.; Piner, R. D.; Colombo, L.; Ruoff, R. S. Transfer of Large-Area Graphene Films for High-Performance Transparent Conductive Electrodes. *Nano Lett.* **2009**, *9*, 4359–4363.

(28) Dreyhaupt, A.; Winnerl, S.; Dekorsy, T.; Helm, M. High-intensity terahertz radiation from a microstructured large-area photoconductor. *Appl. Phys. Lett.* **2005**, *86*, 121114.

(29) Horng, J.; Chen, C.-F.; Geng, B.; Girit, C.; Zhang, Y.; Hao, Z.; Bechtel, H. A.; Martin, M.; Zettl, A.; Crommie, M. F.; Shen, Y. R.; Wang, F. Drude conductivity of Dirac fermions in graphene. *Phys. Rev. B: Condens. Matter Mater. Phys.* **2011**, *83*, 165113.

(30) Xing, G.; Guo, H.; Zhang, X.; Sum, T. C.; Huan, C. H. A. The Physics of ultrafast saturable absorption in graphene. *Opt. Express* **2010**, *18*, 4564–4573.

(31) Gosciniaik, J.; Tan, D. T. H. Theoretical investigation of graphene-based photonic modulators. *Sci. Rep.* **2013**, *3*, 1897.

(32) Chen, H.-W.; Kuo, Y.-h.; Bowers, J. E. 25Gb/s hybrid silicon switch using a capacitively loaded traveling wave electrode. *Opt. Express* **2010**, *18*, 1070–1075.

(33) Liu, M.; Yin, X.; Zhang, X. Double-Layer Graphene Optical Modulator. *Nano Lett.* **2012**, *12*, 1482–1485.

(34) Koester, S. J.; Li, M. High-speed waveguide-coupled graphene-on-graphene optical modulators. *Appl. Phys. Lett.* **2012**, *100*, 171107.

(35) Fallahzad, B.; Lee, K.; Lian, G.; Kim, S.; Corbet, C. M.; Ferrer, D. A.; Colombo, L.; Tutuc, E. Scaling of Al₂O₃ dielectric for graphene field-effect transistors. *Appl. Phys. Lett.* **2012**, *100*, 093112.

(36) Liao, L.; Bai, J.; Cheng, R.; Lin, Y.-C.; Jiang, S.; Qu, Y.; Huang, Y.; Duan, X. Sub-100 nm channel length graphene transistors. *Nano Lett.* **2010**, *10*, 3952–3956.